

Cyclic Adenosine Monophosphate-Enhanced Calvarial Regeneration by Bone Marrow-Derived Mesenchymal Stem Cells on a Hydroxyapatite/Gelatin Scaffold

TianJuan Ju, ZiYi Zhao, LiQiong Ma, WuLi Li, Song Li,* and Jing Zhang*



Cite This: *ACS Omega* 2021, 6, 13684–13694



Read Online

ACCESS |



Metrics & More

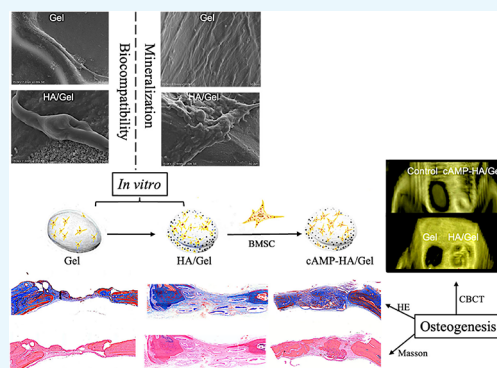


Article Recommendations



Supporting Information

ABSTRACT: Cyclic adenosine monophosphate (cAMP) plays a significant role in inducing new bone formation by mediating various signal pathways. However, cAMP, combined with biomaterials, is rarely investigated to reconstruct calvarial defects. In this study, cAMP was loaded into a hydroxyapatite (HA)/gelatin (Gel) construct and implanted into critical skull defects in rats to evaluate the potential for enhancing skull regeneration. The physiochemical characteristics, the biocompatibility of Gel and HA/Gel scaffolds, and the regenerated bone tissue were assessed. The resulting HA/Gel scaffolds possessed a 3D interconnected porous structure with extensively distributed HA crystals and favorable physiochemical properties. Rat bone marrow-derived mesenchymal stem cells (rBMSCs) within the HA/Gel scaffold showed greater biocompatibility. Compared with the Gel and HA/Gel groups, the cAMP-HA/Gel group revealed the highest bone density, more mature mineralized tissue, and more favorable integration between the new bone and inherent bone as analyzed by cone beam computed tomography and hematoxylin & eosin and Masson staining, respectively. Collectively, our study verified HA/Gel scaffolds as a prospective biomimetic treatment with biocompatibility and the therapeutic potential of cAMP in promoting new bone growth of a skull, which indicates its promise as a growth factor for bone tissue engineering.



INTRODUCTION

There is an increasing demand for regenerating large bone defects that typically result in a permanent deformity or functional deficiency.¹ However, clinically established therapies to restore bone defects, such as autografts, allografts, and demineralized bone matrices, still have some limitations including availability, donor complications, cost, safety, time, and ability to repair large bone defects.² Therefore, satisfactory regenerative treatments that restore the physiological appearance and function as well as provide a sustainable outcome still need to be explored.³

Tissue engineering and regenerative medicine, commonly comprising stem cells, biocompatible scaffolds, and growth factor components, have advantages in promoting newly formed bones derived from patient's stem cells, completely integrating with the existing skeletal system.^{4,5} Hydroxyapatite (HA) is an excellent scaffold among biomaterials for repairing bone defects, given its biocompatibility, osteoconductivity, and lack of a foreign-body response.⁶ HA can strengthen natural bones, making them resistant to crushing, whereas the bioactive effect of HA is still limited by invasion into tissues around the implanted area and poor formability because of their natural stiffness and brittleness.⁷

Incorporating HA into other natural biopolymers, such as gelatin (Gel), is effective in modifying properties of HA and

fabricating high-quality HA bioceramics because a biopolymer can form pore structures to increase the surface area and open space that is beneficial to nutrient delivery and cell ingrowth in bone defects.^{8,9} Furthermore, Gel also promotes the initial cell adhesion based on the presence of the integrin recognition motif Arg-Gly-Asp.¹⁰ Overall, HA/Gel blends are considered promising scaffolds for stimulating bone regeneration.¹¹

A recent study considered the potential of enhanced osteogenic differentiation that was modulated by the cyclic adenosine monophosphate (cAMP) signaling pathway.¹² cAMP, a physiologically important secondary messenger, plays a significant role in transmitting intracellular signals by conveying the cAMP-dependent pathway. cAMP is responsible for inducing osteogenic differentiation by enhancing the osteogenic potential of stem cells from apical papilla and human mesenchymal stem cells (MSCs).^{13,14} Such a mechanism is able to promote the osteogenic effects of MSCs that were further correlated with the cAMP/protein

Received: February 17, 2021

Accepted: May 4, 2021

Published: May 17, 2021



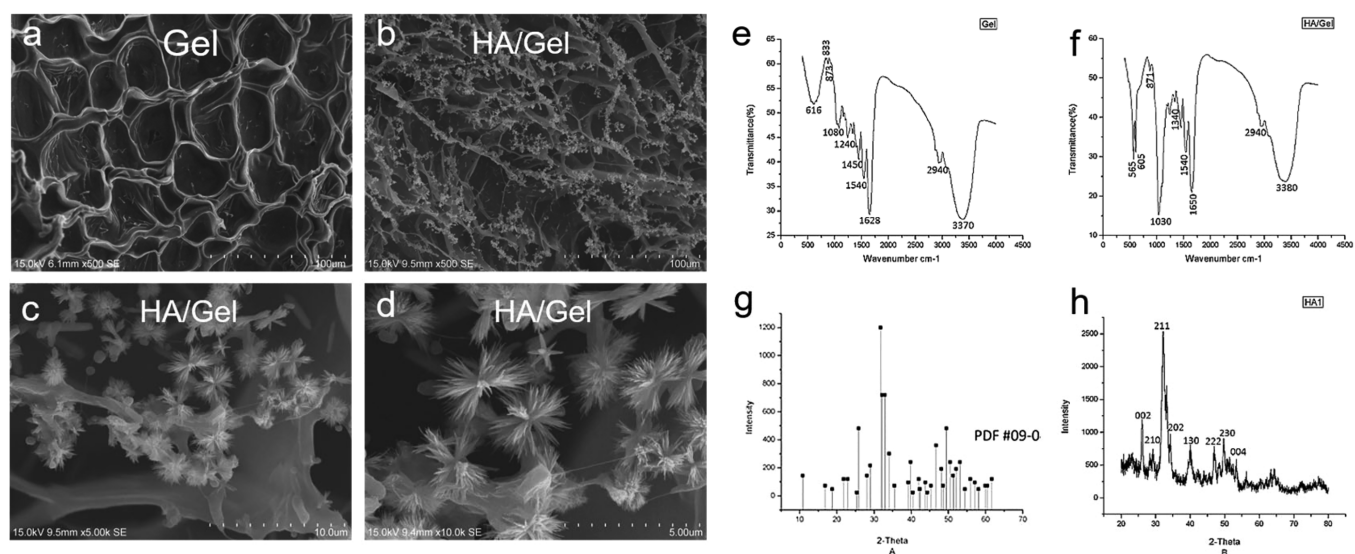


Figure 1. Representative SEM images showing the interconnecting pores, distribution of deposited particles, and shape of (a) Gel and (b–d) HA/Gel scaffolds (original magnification: $\times 500$, $\times 5000$, and $\times 10,000$). (e, f) FTIR analyses of Gel and HA/Gel scaffolds that demonstrate the cross-linking reaction of gelatin and HA. (g) XRD standard card of HA. (h) XRD analysis of HA/Gel showing HA particles deposited on the Gel scaffolds.

Table 1. Elemental Composition and Ca/P Ratio of HA/Gel Studied by EDX

elt.	line	intensity (c/s)	atom %	atomic ratio	conc.	units	error 2-sig	MDL 3-sig
P	Ka	321.64	42.656	1.0000	36.503	wt %	0.447	1.224
Ca	Ka	301.85	57.344	1.3443	63.497	wt %	0.752	2.257
total			100.000		100.000	wt %		

kinase A (PKA) signaling pathway.¹⁵ Activation of cAMP/PKA also promoted osteoblast cell adhesion on biodegradable scaffolds.¹⁶ Additionally, the potential of repairing a mouse femoral fracture was accelerated by the activation of the cAMP/cAMP response element-binding protein (CREB) signaling pathway, which significantly improved the osteopromotive action.¹⁷ However, limited data exists on integrating cAMP with an HA/Gel scaffold for repairing calvarial defects. Therefore, we blended cAMP with HA/Gel scaffolds that were implanted into rat skull defects to evaluate if the exogenous stimulation cAMP enhances the osteogenic differentiation of rat bone marrow-derived mesenchymal stem cells (rBMSCs) to promote the restoration of critical-sized calvarial defects.

RESULTS

Characterization of the Scaffolds. The SEM images of the fabricated Gel and HA/Gel scaffolds are illustrated in Figure 1a–d. The Gel scaffolds showed a smooth surface and abundant interconnecting porous structures, ranging in sizes from 200 to 400 μm (Figure 1a). The HA/Gel group exhibited a large number of HA-like crystals homogeneously deposited on the surface and the pore wall of the Gel scaffolds (Figure 1b). Under high magnification, the crystallites precipitated on the Gel surface well in apatite clusters with relatively uniform morphology and distribution (Figure 1c,d).

FTIR spectral analysis of the Gel scaffolds (Figure 1e) shows the characteristic peaks at 3370, 2940, 1628, 1540, 1450, and 1080 cm^{-1} , which represent the presence of $-\text{OH}$, $-\text{CH}$, $-\text{C}=\text{O}$, $-\text{NH}$, $-\text{CN}$, and $-\text{CO}$ functional groups, respectively. In HA/Gel scaffolds (Figure 1f), the absorption bands at 3380 and 1650 cm^{-1} were characteristic peaks of the $-\text{OH}$ stretching and $\text{C}=\text{O}$ stretching of amide II, while amide

II at 1540 cm^{-1} was coupled with the $\text{N}-\text{H}$ bending and $\text{C}-\text{N}$ stretching. Thus, it was confirmed that the organic phases in the composite were gelatin. The presence of HA on the surface of the composite could be confirmed by the characteristic absorption peaks of $\text{PO}_4^{3-}\text{V}_3$ at 1030 cm^{-1} and the bending vibrations of $\text{P}-\text{O}$ at 565 and 605 cm^{-1} . The peak at 1340 cm^{-1} indicates that a $\text{Ca}-\text{COO}$ bond was formed between the $-\text{COOH}$ species of gelatin and the Ca^{2+} species of HA.

The XRD analyses of reference HA and HA/Gel scaffolds are presented in Figure 1. Compared with the XRD standard card of HA (Figure 1g), the diffraction peaks of HA/Gel (Figure 1h) corresponded well to the (002), (210), (211), (202), (130), (222), (230), and (004) crystal faces of HA, suggesting that the crystalline particles deposited on the scaffolds were HA.

The EDX analysis (Table 1) demonstrated that the crystals deposited on Gel were HA, and the calculated Ca/P ratio was 1.74, which is slightly higher than the theoretical value of 1.67.

The TG curve (Figure 2a) of the HA/Gel scaffolds shows that there were two stages of weight loss in the temperature ranges of 38.6–190.35 and 190.3–610.30 $^{\circ}\text{C}$ with weightlessness rates of 6.909 and 26.40%, respectively, that coincided with the peak of the DTA curve. The mass loss rate of the HA/Gel scaffolds was accelerated, and the amount of loss increased in the second stage of weight loss compared with the first stage in the analysis of the DTA curve. Therefore, the remaining mass of this scaffold was 66.691% at 610.3 $^{\circ}\text{C}$.

As shown in Figure 2b, the degradation rate for the synthesized HA/Gel nanocomposite was the fastest in the first 2 weeks during the cultivation period, and the mass loss quickly reached 12%. Subsequently, the rate diminished and

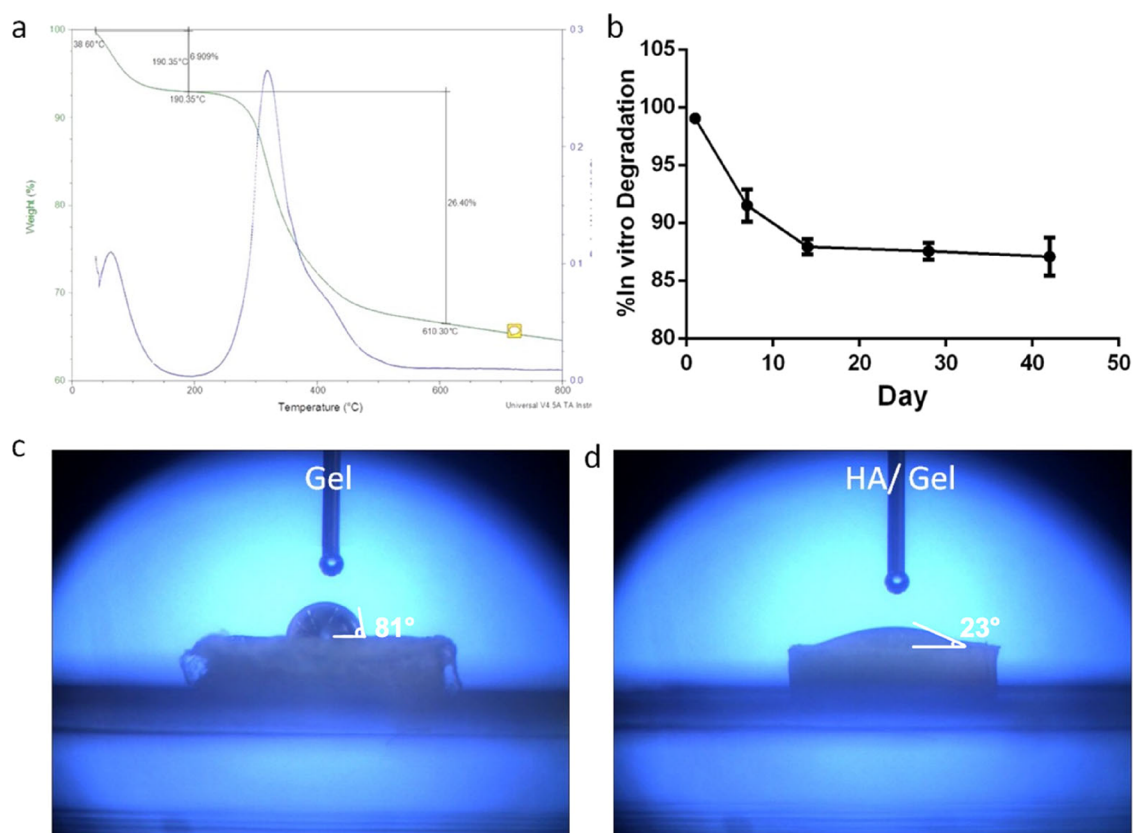


Figure 2. (a) TGA exhibiting the thermal properties of the HA/Gel scaffolds. (b) Degradation curve of the HA/Gel scaffolds. (c, d) Water contact angle analysis showing the hydrophilicity of the Gel and HA/Gel scaffolds.

gradually slowed. The degradation process was continuing slowly, even after 42 days.

The water contact angle analysis done to measure the hydrophilicity of the scaffold surface exhibited that the contact angle value of the Gel scaffold (Figure 2c) was 81°, whereas that of the HA/Gel group was 23°, which was far less than that of Gel and indicated that it possessed great hydrophilic surfaces (Figure 2d).

Assessment of the Cell Morphology, Viability, and Proliferation of rBMSCs Seeded on the Scaffolds. As shown by the SEM images (Figure 3a), the rBMSCs exhibited a spindle shape and were successfully adhered and stretched on both scaffolds (Gel and HA/Gel). In the HA/Gel group (Figure 3a), pseudopodia protruding from the rBMSCs were clearly observed at high magnification, attaching to the surface and extending into the HA particles.

The CCK-8 assay (Figure 3b) was conducted to detect the proliferation of cells in the Gel and HA/Gel scaffolds. After 1 and 3 days of culture, the absorbance values of the Gel scaffold were larger than those of the HA/Gel nanocomposite ($P < 0.05$), while starting from day 5, the proliferation of rBMSCs inside the HA/Gel scaffold was superior to that in the Gel group, and the difference was statistically significant ($P < 0.05$).

Live/dead fluorescence staining (Figure 3c) revealed that the cells in both scaffolds exhibited high levels of cell viability, and the density of rBMSCs increased significantly with time, as shown by the green cells that died by AO. The comparison between the Gel and HA/Gel scaffolds showed that the viable

cell population was similar between both groups after 1, 3, and 7 days of culture.

Evaluation of the Mineralized Tissue Formation within the rBMSC-Seeded Scaffolds. The SEM images (Figure 4a) showed a few, small granular calcified matrices on the rBMSC-seeded Gel after incubation in phosphate-rich CCM for 21 days. Notably, the calcified tissue formed by rBMSCs seeded in the HA/Gel scaffold (Figure 4a) aggregated into a patch shape with nodes, and the cell bodies were partially covered and embedded in the mineralized tissue.

Assessment of the Osteogenic Differentiation Potential of rBMSC-Seeded Scaffolds. The ALP activity (Figure 4b) of the two groups (Gel and HA/Gel) was assessed at different time points (1, 3, 5, and 10 days) to evaluate the role of scaffolds in promoting osteogenic differentiation of rBMSCs. The ALP activity of both groups continued to increase with time; however, the HA/Gel scaffolds had more activity that was significantly different from the Gel ($P < 0.05$ for 3, 5, and 10 days).

The expression of osteogenic-related genes based on qPCR analysis (Figure 4c) was observed in both scaffolds (Gel and HA/Gel). Specifically, the rBMSCs seeded into HA/Gel more favorably promoted the upregulation of all osteogenic-related gene expression compared with the rBMSCs inside Gel scaffolds, including ALP, Col, OCN, and Runt-related transcription factor 2 (RUNX2). Among them, those of ALP and OCN in HA/Gel were statistically significant ($P < 0.05$). Notably, compared with the Gel group, the expression of RUNX2 was much greater in HA/Gel ($P < 0.001$).

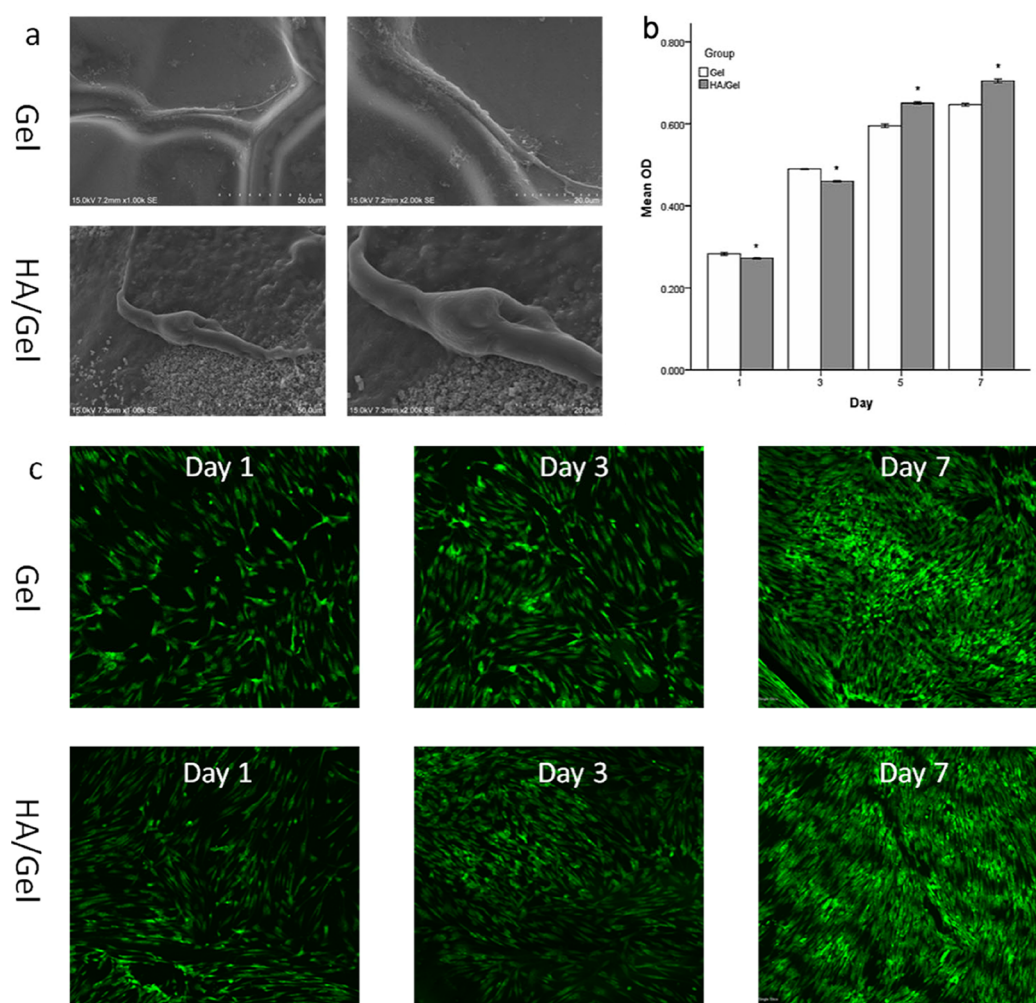


Figure 3. (a) Representative SEM images showing cell adhesion and spreading within Gel and HA/Gel scaffolds after 1 week of culture (original magnification: $\times 1000$ and $\times 2000$). (b) CCK-8 results showing cell proliferation of rBMSCs seeded on Gel and HA/Gel scaffolds for 1, 3, 5, and 7 days. (c) AO/PI staining done to evaluate cell viability of BMSCs inside Gel and HA/Gel scaffolds after 1, 3, and 7 days of culture.

Regeneration of Bone-like Tissues in Calvarial Defects *In Vivo*. The cone beam computed tomography (CBCT) results (Figure 5a) evaluated the regenerated bone defect area after the scaffolds were implanted for 12 weeks. The 3D images (Figure 5a) revealed that the volume of the defect area in the Gel group after 12 weeks was nearly the same as that in the control group, while the HA/Gel and cAMP-HA/Gel groups showed obvious newly formed bone tissues. In particular, the bone defect in cAMP-HA/Gel had basically healed. The axial images (Figure 5a) show consistent results. There was regenerated bone tissue integrating with the old bone at both ends in the HA/Gel and cAMP-HA/Gel groups compared with the Gel and control groups, in which no connections between the new and old bone existed. Favorably, the bone is complete in the cAMP-HA/Gel group, and the thickness of the regenerated bone was very similar to that of the inherent bone, while the regenerated bone in HA/Gel was uneven and incomplete. BMD (bone mineral density) values of the blank control, Gel, HA/Gel, and cAMP-HA/Gel groups were $-(165.33 \pm 11.68)$, $-(129.67 \pm 14.58)$, $+(78.33 \pm 12.23)$, and $+(147.26 \pm 13.42)$, respectively. The BMD (Figure 5b) in the HA/Gel and cAMP-HA/Gel groups were greater ($P < 0.001$) than that in the control and Gel groups. Notably, the BMD in the cAMP-HA/Gel group was the

highest among the four groups ($P < 0.001$), while there was no statistical significance between the control and Gel groups.

As shown in the histological sections stained with HE (Figure 6) and Masson (Figure 7) after implantation in the defect area for 12 weeks, there was no continuous connective tissue between the regenerated tissue, collagenous fibers, and natural bone in the control group. In the Gel group, only sparse mineralized tissue and large amounts of connective tissue were observed. Alternatively, a complete and continuous integration was observed in both HA/Gel and cAMP-HA/Gel groups: the HA/Gel group exhibited a mixture of some mineralized tissue and a large amount of extracellular matrix. Interestingly, the degree of mineralized tissue in the cAMP-HA/Gel was more mature, which was very close to the inherent bone, and the fibrous tissue was less than that of HA/Gel. HE staining (Figure 7) revealed uniform osteoprogenitor cell distribution and favorable continuity of newly formed bone tissue in the defect areas of both experimental groups (HA/Gel and cAMP-HA/Gel). The cAMP-HA/Gel group showed more abundant new bone and bone islands. Masson staining further illustrated that newly formed bone tissue rich in collagen was gradually mineralized into mature bone tissue that presented as red in the staining of cAMP-HA/Gel. The schematic diagram depicting the conceptual framework is shown in Figure 8.

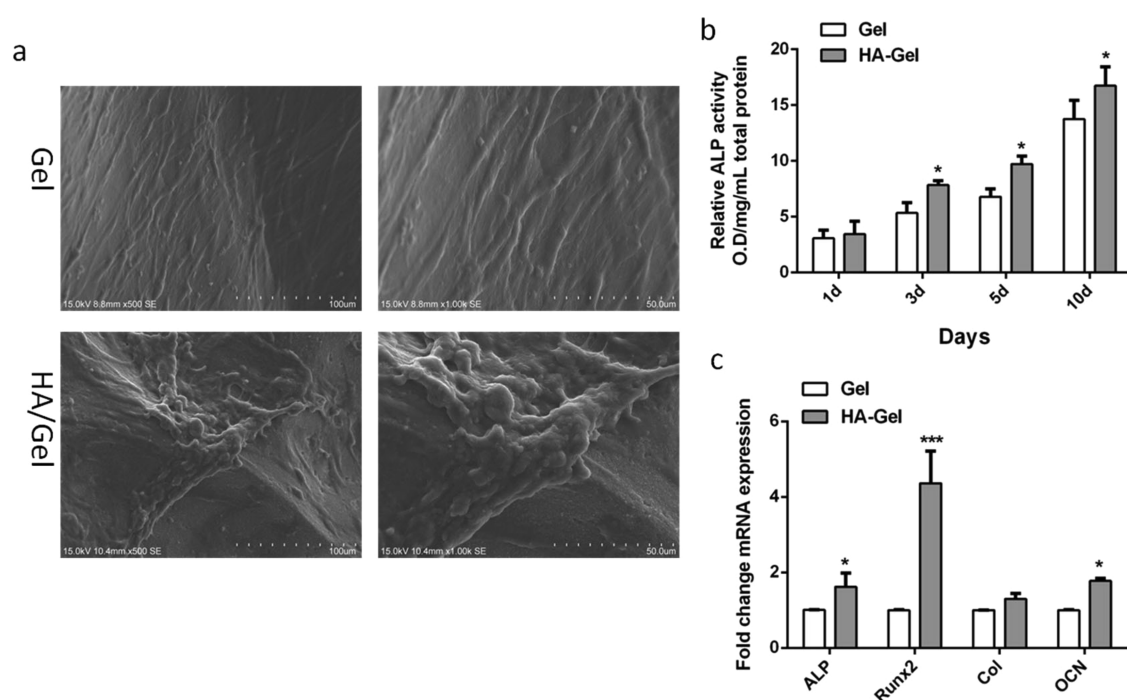


Figure 4. (a) Formation of mineralized tissue within Gel and HA/Gel as illustrated by representative SEM images after 21 days of culture (original magnification: $\times 500$ and $\times 1000$). (b) ALP activity showing the potential of cell differentiation after rBMSCs were seeded to Gel and HA/Gel scaffolds for 1, 3, 5, and 10 days. (c) Real-time PCR analysis of the expression of osteogenic-related genes (ALP, RUNX2, Col, and OCN) in rBMSC-loaded Gel and HA/Gel scaffolds after 21 days of culture.

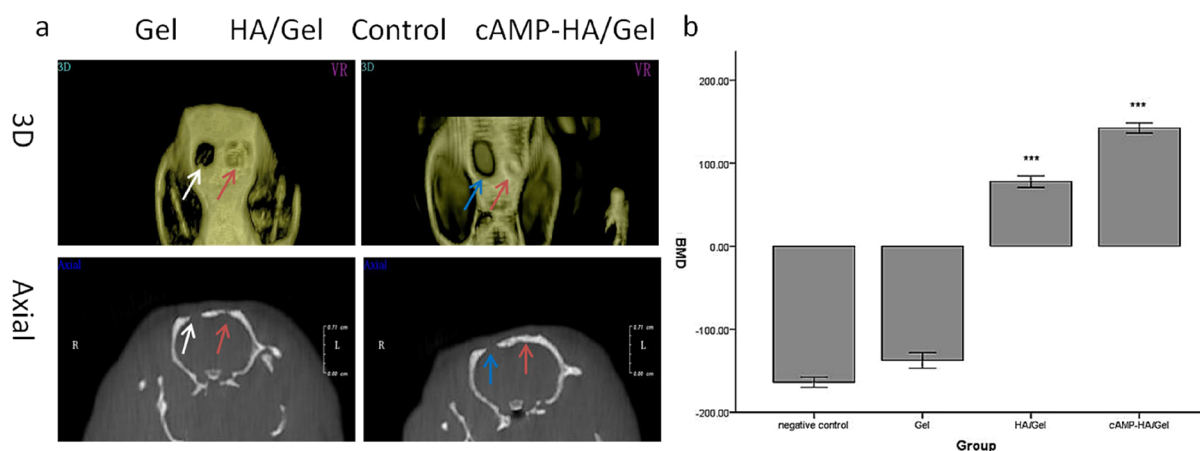


Figure 5. (a) 3D and axial images of Gel, HA/Gel, and cAMP-HA/Gel scaffolds implanted into skull defects for 12 weeks. The blank group acted as a control. The white and blue arrows indicate Gel and control groups, respectively. The red arrow refers to the HA/Gel and cAMP-HA/Gel scaffolds. (b) BMD statistical analysis of the skull defects of the control, HA/Gel, BMSC-cAMP HA/Gel, and Gel scaffolds implanted into bone defects for 12 weeks, respectively (** $^*P < 0.001$ cAMP-HA/Gel group compared with the control, Gel, and HA/Gel; ** $^*P < 0.001$ HA/Gel compared with the control and Gel groups).

DISCUSSION

Recently, there are many research studies exploring the effects of bioactive inorganic/organic–polymer composites on bone regeneration. For example, the chitin/HA composites can remarkably contribute cell adhesion and bone healing, which showed that the 1.5 cm-radius defect in rabbits was almost cured completely in 3 months with the participation of growth factors and cells.¹⁸ In 2017, the great potential of silk fibroin/HA nanoparticle composite hydrogels in improving osteogenic differentiation has been demonstrated, which promoted the activity of ALP and the accumulation of calcium *in vitro*.¹⁹ Gel has been widely blended with multiple polymers to fabricate

promising scaffolds for application in bone tissue engineering. The superiority of Gel is because of its favorable biocompatibility, biodegradability, and noninflammatory reaction.^{20,21} Gel can also act as a delivery vehicle for growth factors and cells to greatly enhance bone regeneration.^{22,23} However, there are some drawbacks, including the inability to maintain cell viability and cell spread on its surface even with an adequate extracellular environment and inadequate mechanical strength that can be enhanced by adding stronger materials.³ From the perspective of bionics, HA and gelatin improve interactions between cells and scaffolds as well as simulate the composition and structure of natural bone. Therefore, HA and Gel were

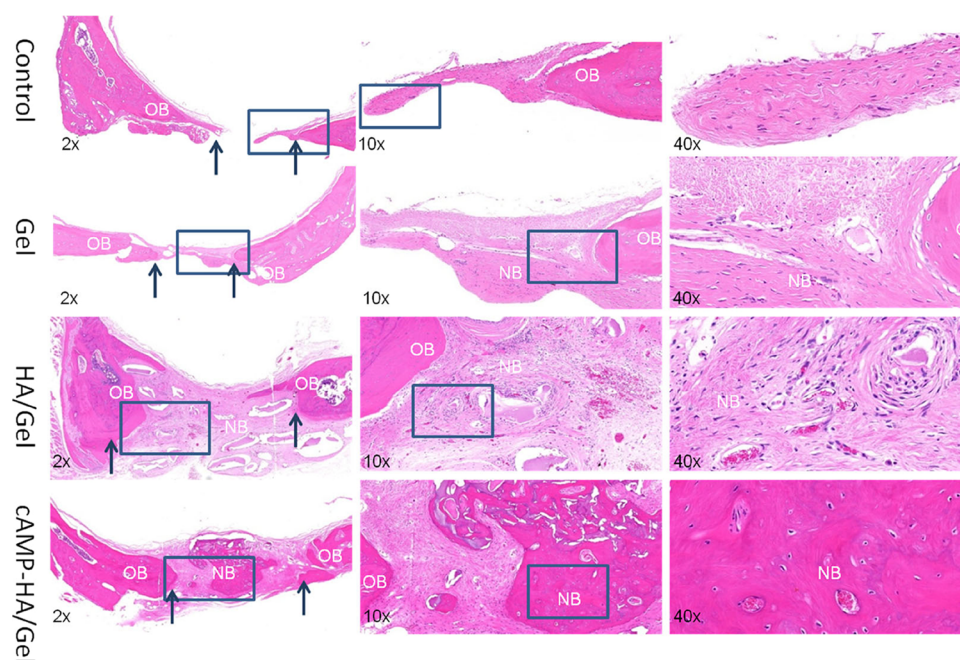


Figure 6. H&E-stained histological samples obtained 12 weeks post implant from rats that received blank control, Gel, HA/Gel, and cAMP-HA/Gel treatment to evaluate the regenerated bone defect area. The arrows indicate the boundary between the old and new bone (original magnification: $\times 2$, $\times 10$, and $\times 40$; OB, old bone; NB, new bone).

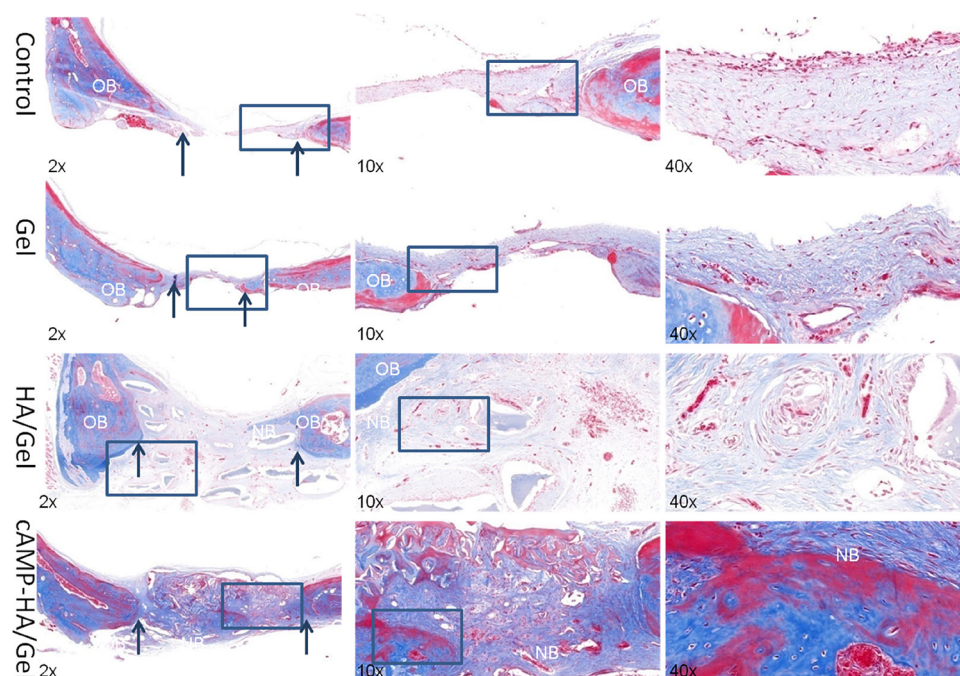


Figure 7. Masson-stained histological samples obtained 12 weeks post implant from rats that received blank control, Gel, HA/Gel and cAMP-HA/Gel treatment to evaluate the regenerated bone defect area. The arrows indicate the boundary between the old and new bone (original magnification: $\times 2$, $\times 10$, and $\times 40$; OB, old bone; NB, new bone).

selected to synthesize scaffolds to evaluate their physiochemical properties and roles in inducing osteogenic differentiation of rBMSCs.

There are many important parameters affecting the biological properties of scaffolds, such as the porous surface, 3D pore interconnectivity, and porosity.²⁴ Hulbert et al. identified that porous implants around tissue facilitate defect healing and display thinner fibrous encapsulation compared with non-porous implants.²⁵ In this study, the pore size of the HA/Gel

constructs was approximately $200 \mu\text{m}$, which is beneficial for osteogenesis. Macropores (pores, $>100 \mu\text{m}$) play a significant role in accelerating cell and ion transport.²⁶ A relatively high porosity of 70–75% with interconnectivity in this paper allows cells to distribute uniformly and the scaffolds to absorb nutrition from the microenvironment.²⁷ Additionally, fibrous tissues and blood vessels can infiltrate scaffolds with an interconnected structure.²⁵ Although the scaffold can provide a 3D structure for a defect, it is still a foreign material in tissue

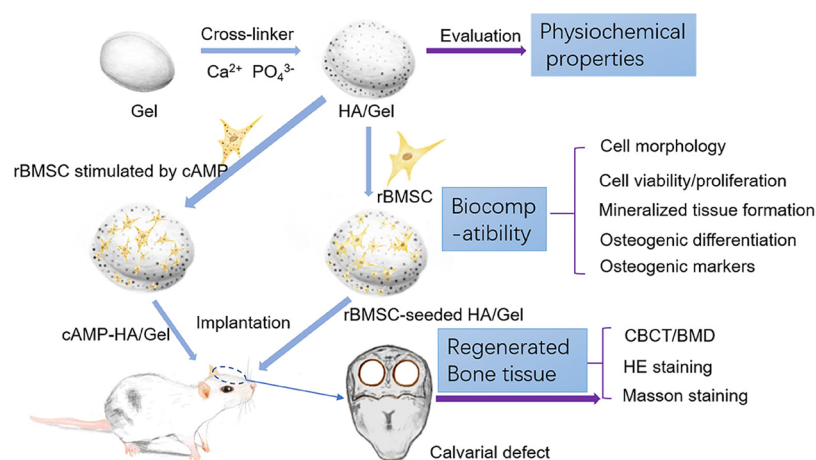


Figure 8. Schematic diagram depicting the conceptual framework.

that should degrade as the bone cells proliferate and the healing process occurs.²⁸ Degradation (Figure 2b) experiments showed that the mass loss of the HA/Gel scaffold reached 13% after 42 days, indicating biodegradability and the ability to support tissue in the early stage of bone defect repair. Moreover, hybrid scaffolds should maintain thermal stability at body temperature and during sterilization processes. TGA (Figure 2a) inferred that the incorporation of HA particles into the Gel enhanced the scaffold thermal stability, as the HA/Gel constructs in the present study started to lose weight at 190.35 °C while Gel films lost weight at 160 °C.²⁹ The theoretical basis is that the HA nanoparticles can act as a thermal dielectric and barrier of volatile compounds produced by decomposition of polymers.³⁰ Therefore, the HA/Gel scaffold fabricated in this study was conducive to the transmission of body fluids and nutritional factors as well as cell growth and tissue regeneration, given its similarity to the pore size and porosity of human cancellous bone.

In addition to the above properties of the hybrid scaffolds, the particle size of the bionic matrix also affects the interaction between biomaterials and cells.³¹ Previous studies identified that HA particles larger than 100 nm were beneficial to promoting cell growth, and the greatest cell compatibility is attained when the sizes of the cells and biomaterials are equivalent.^{32,33} In the present study, HA/Gel scaffolds induced the deposition of HA crystals with controllable sizes of 100–200 nm that were conducive to cell attachment and proliferation. ALP and RUNX2 are two major osteogenic differentiation genes. ALP activity is accepted as an early osteogenic differentiation marker of cells, and a higher level of ALP expression represents a more differentiated phase.³⁴ RUNX2 is expressed in osteoblast lineage cells and is responsible for regulating the initiation of osteoblast differentiation during development and bone formation.³⁵ In our study, ALP (Figure 4b) and qPCR analyses (Figure 4c) demonstrated that the HA/Gel scaffolds significantly facilitated ALP secretion and dramatically strengthened the expression of osteogenic-related genes (RUNX2), respectively. Therefore, the HA/Gel scaffold possessed excellent biological properties and the potential to induce BMSC osteogenic differentiation.

Several emerging growth factors have been established for promoting osteogenesis, such as BMP and cAMP. In the present study, cAMP was loaded into HA/Gel scaffolds implanted into rat calvarial defects for 12 weeks to evaluate whether it promoted the restoration of critical-sized calvarial

defects. According to CBCT and HE staining, the cAMP-HA/Gel group showed the highest BMD ($P < 0.001$) of regenerated bone, more bone islands, and more mature mineralized tissues that are very close to the inherent bone. Masson staining (Figure 7) further demonstrated that the newly formed bone tissue rich in collagen was gradually mineralized into mature bone tissue presented as red in the staining of cAMP-HA/Gel. These results suggested that the regeneration of the bone in calvarial defects was remarkably improved after cAMP was introduced to HA/Gel scaffolds, which is consistent with other studies. In 2019, Zhang et al. demonstrated that the activator of cAMP enabled interfering of transforming growth factor beta 1 signaling to stimulate stem cells of the apical papilla (SCAP) odonto/osteogenic differentiation.³⁶ The cAMP/PKA/CREB signaling pathway is an important mechanism of the role of cAMP in inducing osteogenic differentiation. PKA stimulated by cAMP promotes the release of catalytic subunits to activate osteogenic gene expression, such as BMP2, by phosphorylating the cAMP/CREB. BMP2 also participates in osteogenesis, osteogenic markers, and bone formation.³⁷ A previous study also reported that the elevation of the intracellular cAMP level and activation of the phosphorylation of the cAMP/CREB enhanced mouse femoral fracture repair by increasing the bone strength.¹⁷ Additionally, cAMP mediated the activation of MAPK signaling and elicited osteogenic differentiation, which correlates with the upregulation of RUNX2 and other osteogenesis-related genes.³⁸ Furthermore, cAMP promotes vascular calcification by stimulating the osteoblast-like differentiation of calcifying vascular cells.³⁷

Alternatively, a previous study reported that cAMP inhibited osteogenic differentiation in rodent cells, as evidenced by the blocked expression of osteogenic genes such as ALP and type 1 collagen. It is further suggested that the inhibited role may be attributed to the species discrepancy in response to various osteogenic signals.³⁹ In addition, an excessive and sustained increase in cAMP in osteoblasts also suppressed osteoblast differentiation as cAMP can activate adenylyl cyclase to degrade Cbfa1, which is important for differentiation of osteoblastic cells.⁴⁰

CONCLUSIONS

The present study identified the role of cAMP in HA/Gel scaffolds in promoting the restoration of calvarial defects, suggesting that it may be a promising osteoinductive factor for

bone tissue engineering. The physiochemistry properties of HA/Gel scaffolds were further confirmed.

MATERIALS AND METHODS

Synthesis of HA/Gel Scaffolds. HA was blended with gelatin via ion coprecipitation to prepare HA/Gel scaffolds. To prepare the HA/Gel scaffold, 1.25 g of Gel powder (Sigma-Aldrich, Wisconsin, USA) was first dissolved in 50 mL of deionized water and heated to dissolution to produce a 2.5% aqueous solution of gelatin. The solution was cooled at 4 °C to form a solid hydrogel. Then, 0.5 g of 1-(3-dimethylamino-propyl)-3-ethylcarbodiimide hydrochloride powder (EDC; Sigma) and 0.16 g of *N*-hydroxysuccinimide powder (NHS; Sigma) were dissolved in 50 mL of 90% absolute ethanol, and the solution was stirred to prepare the cross-linking agent. The hydrogel was cut into a cylinder with a diameter of 5 mm and a thickness of 3 mm. The hydrogel was then cross-linked at 4 °C overnight and rinsed thoroughly with deionized water. The prepared Gel hydrogel material was alternately added to a phosphate solution (PO_4^{3-} , 0.13 mol/L, pH \approx 7.0) and calcium solution (Ca^{2+} , 0.26 mol/L, pH \approx 7.0). The solution was stirred and soaked for 2 h, and then the materials were soaked with deionized water in multiple intervals for 2–3 days. Finally, Gel and HA/Gel scaffolds were obtained after freezing the material at –20 °C and freeze-drying for 48 h.

Characterization of the HA/Gel Scaffolds. *Scanning Electron Microscopy (SEM).* The freeze-dried composite scaffolds were trimmed into small pieces and attached to a round metal plate with conductive adhesive. After coating with gold, the micromorphology, pore size, and other structures of the scaffolds were observed with a Sirion 200 environmental scanning electron microscope (SEM, FEI, Sirion 200, USA).

Fourier Transform Infrared (FTIR) Spectroscopic Analysis. To determine the cross-linking reaction of Gel and glutaraldehyde, the scaffolds were crushed into powder and analyzed using an FTIR spectrometer (Nicolet 8700 Thermo Scientific Instrument Co., Friars Drive Hudson, USA). The infrared spectra of the samples were measured at wavenumbers ranging from 4000 to 400 cm^{-1} . The transmittance value was determined according to the wavelength to identify the vibration of different chemical bonds.

X-ray Diffraction (XRD) Analysis. The freeze-dried HA/Gel scaffold was crushed into powder and analyzed using an X-ray diffractometer (X'Pert Pro, Philips Almelo, Netherlands) from 10 to 20° at 2 θ to identify the crystalline particles on the biomaterials.

Energy-Dispersive X-ray (EDX) Analysis. SEM equipped with EDX was done to investigate the elemental composition of the HA/Gel scaffolds, operating with conducted silver-sputtered surfaces.

Thermogravimetric Analysis (TGA). The thermal properties of the composites were evaluated by thermogravimetric analysis (TGA) and differential thermal analysis (DTA; TA Instruments Inc. SDTQ600, USA) at a heating rate of 20 °C/min up to 800 °C in a stream of dry nitrogen purge (50 mL/min).

Degradation. The *in vitro* degradation of the HA/Gel cross-linked scaffolds was assessed by immersing samples with a thickness of 2 mm and diameter of 5 mm in 15 mL of PBS at pH 7.4 and 37 °C. See the [Supporting Information](#) for the detailed information.

Water Contact Angle Analysis. Drop shape analysis (DSA 100, KR \ddot{u} ss, Germany) was done to measure the water

contact angles of the scaffolds at room temperature. A 3 μL drop of deionized water was placed on the surface of the Gel and HA/Gel scaffolds and immediately photographed.

Rat BMSC Culture. rBMSCs were isolated from the femurs of male Sprague–Dawley rats (100 \pm 5 g, 4 weeks old, provided by Anhui Medical University) as previously described.⁴¹ Animal protocols were performed according to international regulations. The methods of rBMSC culture are described in the [Supporting Information](#).

Cell Seeding and Evaluation of Cell Morphology, Attachment, Viability, and Proliferation. The Gel and HA/Gel scaffolds were first soaked in a complete culture medium (CCM) containing 10% FBS at 37 °C in a 5% CO_2 , saturated humidity environment for 3 days. Most of the CCM was removed such that the scaffold could be inoculated with cells when the materials were slightly dry. Each scaffold was loaded with passage 2 rBMSCs at a high concentration of 2×10^5 cells/20 μL . The scaffold was initially incubated at 37 °C in a 5% CO_2 saturated humidity for 30 min, after which an appropriate amount of CCM was added. The CCM was changed every 2 days until the rBMSC-seeded Gel (Gel) and rBMSC-seeded HA/Gel scaffolds (HA/Gel) were obtained.

Cell Seeding. The methods of seeding rBMSCs into Gel and HA/Gel scaffolds are described in the [Supporting Information](#).

Observation of the Initial Cell Attachment and Morphological Characteristics by SEM. For SEM observation, the Gel and HA/Gel scaffolds were fixed with 2.5% glutaraldehyde for 24 h, rinsed with PBS, dehydrated with an ethanol gradient to reach the critical drying point, and observed by SEM.

Assessment of the Cell Viability by Live/Dead Staining. To determine the cell viability, the Gel and HA/Gel scaffolds were stained with acridine orange and propidium iodide nuclei dyes (AO/PI) and observed under a confocal microscope (Leica Microsystems, Wetzlar, Germany). The viability assay was conducted per manufacturer's instruction.

Assessment of the Cell Proliferation by CCK-8. The proliferation of rBMSCs on the composite scaffolds was investigated by CCK-8 assay, which is described in detail in the [Supporting Information](#).

Evaluation of the Mineralized Tissue Formation within the Gel and HA/Gel Scaffolds. To evaluate the formation of mineralized tissue, the Gel and HA/Gel constructs were cultured with CCM supplemented with 5 mM β -glycerophosphate as an external phosphate source. The medium was changed every 2 days for a total of 21 days. Both scaffolds were examined by SEM after 21 days.

Evaluation of the Osteogenic Differentiation Potential of the Scaffolds. *Evaluation of the Osteogenic Differentiation Potential of the Scaffold Alkaline Phosphatase (ALP).* The potential of rBMSC differentiation was evaluated by alkaline phosphatase (ALP). Afterward, rBMSCs were seeded onto the Gel and HA/Gel scaffolds and cultured for 1, 3, 5, and 10 days. Following culturing, the scaffolds were washed three times with PBS and incubated with 1% Triton X-100 at 4 °C for 30–40 min. The activity of ALP after cocultivation of the scaffolds and rBMSCs was evaluated according to the manual of the enzyme detection kit (Bioengineering-Institute, Nanjing, China).

Real-Time Reverse-Transcription Polymerase Chain Reaction Analysis (RT-PCR). To evaluate the expression of osteogenic markers by qPCR, rBMSCs were seeded onto Gel and HA/Gel scaffolds and cultured for 21 days. A PureLink RNA Micro Kit (Invitrogen) and a Superscript First-Strand

Synthesis Kit (Invitrogen) were used to isolate the RNA from the cells and synthesize cDNA according to the manufacturer instructions, respectively. qPCR reactions were performed with an SYBR Green Real-Time PCR Master Mix (Applied Biosystems, Foster City, CA, USA) and analyzed with a Step One Plus thermal cycler starting with two incubation steps at 50 °C for 2 min and 95 °C for 2 min for 40 cycles. The $2^{-\Delta\Delta C_t}$ method was used for relative quantification. The results were normalized to the GAPDH mRNA levels and expressed as relative fold changes.

Evaluation of Bone-like Mineralized Tissue Formation inside the rBMSC-Seeded Scaffolds *In Vivo*. In this experiment, the rBMSC-seeded HA/Gel scaffolds (HA/Gel) were prepared as described above. Three experimental groups were used: the rBMSC-seeded Gel scaffolds (Gel), HA/Gel scaffolds, and rBMSCs stimulated by cAMP-seeded HA/Gel scaffolds (cAMP-HA/Gel scaffolds). A blank was used as a control.

Preparation of the cAMP-HA/Gel Scaffolds. To prepare the cAMP-HA/Gel scaffolds, the rBMSCs were first seeded onto the HA/Gel constructs and then cultured with CCM for 3 days. The medium was changed every 2 days. The rBMSC-seeded HA/Gel scaffolds were then incubated with CCM supplemented with 5 mM β -glycerophosphate and cAMP for 2 weeks at 37 °C in 5% CO₂. The Gel and HA/Gel constructs were exposed to the same conditions without cAMP. The constructs were then implanted into the rat calvarial defects.

Implantation of the Scaffolds. Twelve male SD rats (approximately 200 g in weight, provided by the Animal Experimental Center of Anhui Medical University in accordance with ethical requirements) were randomly divided into four groups, blank, Gel, HA/Gel, and cAMP-HA/Gel groups, respectively. Two calvarial defects were made in each rat. Then, the above scaffolds were implanted. All animals were injected with 3.5 mL/kg 10% sterilized chloral hydrate into the abdomen for general anesthesia. A sagittal incision of approximately 2 cm was made in the middle of the forehead of the rat, and the skin and subcutaneous tissue were bluntly separated. The periosteum was peeled off to fully expose the skull. The exposed bones were ground with an electric drill while rinsing with 4 °C sterile physiological saline to cool the site, resulting in a cylindrical defect with a diameter of 5 mm and a depth of approximately 3 mm. During the operation, the socket was not drilled too deep to avoid damage to the dura. All animals used in this study and the experimental operation complied with and were approved by the ethics committee of Anhui Medical University. The HA/Gel, cAMP-HA/Gel, and Gel (5 mm in diameter, 3 mm in thickness) scaffolds were implanted into the defect areas. The incision was sutured, and 200,000 U of penicillin was injected into the lateral thigh muscles on the day of surgery and 3 days after surgery. The rats were fed in their cages normally.

Evaluation of the Bone Density by CBCT. Twelve weeks after surgery, the rats were sacrificed by intraperitoneal injection of excessive 10% chloral hydrate. CBCT was then done to measure the bone density and observe the restoration of the calvarial bone defects. The average BMD of each rat was obtained by measuring the junction of the new bone and both ends of the bone defect and the center of the defected areas.

Histological Assessment of Bone Regeneration by Hematoxylin & Eosin and Masson Trichrome Staining. After the radiographs were taken, the skin and soft tissues on the skull were removed, and the obtained tissues were

decalcified with 10% EDTA for 15 days. The decalcified specimens were sent to Sevier Biotech Co. Ltd. for HE and Masson staining. The slices were observed with an intelligent upright fluorescence microscope to evaluate the repair and healing of the bone defect.

Statistics. SPSS 17.0 was used for statistical analysis, and data were expressed as means \pm standard deviations. One-way ANOVA was used for multiple comparisons among groups.

■ ASSOCIATED CONTENT

Supporting Information

The Supporting Information is available free of charge at <https://pubs.acs.org/doi/10.1021/acsomega.1c00881>.

Representative flow cytometry histograms showing the expression of MSC surface markers (CD90 and CD29) and vascular endothelial cell markers (CD45 and CD11b); materials and methods including degradation, establishment of the rat BMSC culture, cell seeding, assessment of cell proliferation by CCK-8, immunophenotypic profiles of rBMSC cultures; and results including immunophenotypic profiles of BMSC cultures (PDF)

■ AUTHOR INFORMATION

Corresponding Authors

Song Li – Stomatological Hospital and College, Key Lab. of Oral Diseases Research of Anhui Province, Anhui Medical University, Hefei, Anhui 230032, China; Phone: +86 18155116922; Email: 3197053337@qq.com

Jing Zhang – Stomatological Hospital and College, Key Lab. of Oral Diseases Research of Anhui Province, Anhui Medical University, Hefei, Anhui 230032, China; orcid.org/0000-0002-2774-8110; Phone: +86 15055153571; Email: zhangjinglh817@126.com

Authors

TianJuan Ju – Stomatological Hospital and College, Key Lab. of Oral Diseases Research of Anhui Province, Anhui Medical University, Hefei, Anhui 230032, China

ZiYi Zhao – Stomatological Hospital and College, Key Lab. of Oral Diseases Research of Anhui Province, Anhui Medical University, Hefei, Anhui 230032, China

LiQiong Ma – Stomatological Hospital and College, Key Lab. of Oral Diseases Research of Anhui Province, Anhui Medical University, Hefei, Anhui 230032, China

WuLi Li – Stomatological Hospital and College, Key Lab. of Oral Diseases Research of Anhui Province, Anhui Medical University, Hefei, Anhui 230032, China

Complete contact information is available at: <https://pubs.acs.org/10.1021/acsomega.1c00881>

Notes

The authors declare no competing financial interest.

#The authors declare no competing financial interest and Figure ⁸ is available for free.

■ ACKNOWLEDGMENTS

This study was supported by the National Natural Science Foundation of China (no. 81400497), the Health and Medical Research Fund (HMRF) (no. 06171376) of the Food and Health Bureau of the Hong Kong Government, the Natural Science Foundation of Anhui Province (no. 2008085MH255),

and the doctoral foundation of Anhui Medical University (no. XJ201632).

REFERENCES

- (1) Leach, J. K.; Mooney, D. J. Bone engineering by controlled delivery of osteoinductive molecules and cells. *Expert Opin. Biol. Ther.* **2004**, *4*, 1015–1027.
- (2) Shibuya, N.; Jupiter, D. C. Bone graft substitute: allograft and xenograft. *Clin. Podiatr. Med. Surg.* **2015**, *32*, 21–34.
- (3) Tang, D.; Tare, R. S.; Yang, L.-Y.; Williams, D. F.; Ou, K.-L.; Oreffo, R. O. Biofabrication of bone tissue: approaches, challenges and translation for bone regeneration. *Biomaterials* **2016**, *83*, 363–382.
- (4) Hartman, E. H. M.; Vehof, J. W. M.; Spauwen, P. H. M.; Jansen, J. A. Ectopic bone formation in rats: the importance of the carrier. *Biomaterials* **2005**, *26*, 1829–1835.
- (5) Howard, D.; Buttery, L. D.; Shakesheff, K. M.; Roberts, S. J. Tissue engineering: strategies, stem cells and scaffolds. *J Anat* **2008**, *213*, 66–72.
- (6) Zhou, H.; Lee, J. Nanoscale hydroxyapatite particles for bone tissue engineering. *Acta Biomater.* **2011**, *7*, 2769–2781.
- (7) Sun, F.; Zhou, H.; Lee, J. Various preparation methods of highly porous hydroxyapatite/polymer nanoscale biocomposites for bone regeneration. *Acta Biomater.* **2011**, *7*, 3813–3828.
- (8) Sakamoto, M.; Nakasu, M.; Matsumoto, T.; Okihana, H. Development of superporous hydroxyapatites and their examination with a culture of primary rat osteoblasts. *J Biomed Mater Res A* **2007**, *82*, 238–242.
- (9) Yaylaoglu, M. B.; Korkusuz, P.; Ors, U.; Korkusuz, F.; Hasirci, V. Development of a calcium phosphate-gelatin composite as a bone substitute and its use in drug release. *Biomaterials* **1999**, *20*, 711–719.
- (10) Schönwälder, S. M. S.; Bally, F.; Heinke, L.; Azucena, C.; Bulut, O. D.; Heißler, S.; Kirschhöfer, F.; Gebauer, T. P.; Neffe, A. T.; Lendlein, A.; Brenner-Weiß, G.; Lahann, J.; Welle, A.; Overhage, J.; Wöll, C. Interaction of human plasma proteins with thin gelatin-based hydrogel films: a QCM-D and ToF-SIMS study. *Biomacromolecules* **2014**, *15*, 2398–2406.
- (11) Kim, H.-W.; Kim, H.-E.; Salih, V. Stimulation of osteoblast responses to biomimetic nanocomposites of gelatin-hydroxyapatite for tissue engineering scaffolds. *Biomaterials* **2005**, *26*, 5221–5230.
- (12) Kuttappan, S.; Jo, J. I.; Menon, D.; Ishimoto, T.; Nakano, T.; Nair, S. V.; Tabata, Y.; Nair, M. B. ONO-1301 loaded nanocomposite scaffolds modulate cAMP mediated signaling and induce new bone formation in critical sized bone defect. *Biomater. Sci.* **2020**, *8*, 884–896.
- (13) Yang, D.-C.; Tsay, H.-J.; Lin, S.-Y.; Chiou, S.-H.; Li, M.-J.; Chang, T.-J.; Hung, S.-C. cAMP/PKA regulates osteogenesis, adipogenesis and ratio of RANKL/OPG mRNA expression in mesenchymal stem cells by suppressing leptin. *PLoS One* **2008**, *3*, No. e1540.
- (14) Zhang, J.; Zhao, I. S.; Yu, O. Y.; Li, Q.; Mei, M. L.; Zhang, C.; Chu, C. H. Layer-by-layer self-assembly polyelectrolytes loaded with cyclic adenosine monophosphate enhances the osteo/odontogenic differentiation of stem cells from apical papilla. *J. Biomed. Mater. Res.* **2021**, *109*, 207–218.
- (15) Siddappa, R.; Martens, A.; Doorn, J.; Leusink, A.; Olivo, C.; Licht, R.; van Rijn, L.; Gaspar, C.; Fodde, R.; Janssen, F.; van Blitterswijk, C.; de Boer, J. cAMP/PKA pathway activation in human mesenchymal stem cells in vitro results in robust bone formation in vivo. *Proc. Natl. Acad. Sci. U. S. A.* **2008**, *105*, 7281–7286.
- (16) Lo, K.-W.; Ashe, K. M.; Kan, H. M.; Lee, D. A.; Laurencin, C. T. Activation of cyclic amp/protein kinase: a signaling pathway enhances osteoblast cell adhesion on biomaterials for regenerative engineering. *J. Orthop. Res.* **2011**, *29*, 602–608.
- (17) Zhang, Z.-R.; Leung, W.; Li, G.; Kong, S.; Lu, X.; Wong, Y.; Chan, C. Osteole Enhances Osteogenesis in Osteoblasts by Elevating Transcription Factor Osterix via cAMP/CREB Signaling In Vitro and In Vivo. *Nutrients* **2017**, *9*, 588.
- (18) Duan, B.; Shou, K.; Su, X.; Niu, Y.; Zheng, G.; Huang, Y.; Yu, A.; Zhang, Y.; Xia, H.; Zhang, L. Hierarchical Microspheres Constructed from Chitin Nanofibers Penetrated Hydroxyapatite Crystals for Bone Regeneration. *Biomacromolecules* **2017**, *18*, 2080–2089.
- (19) Kim, M. H.; Kim, B. S.; Lee, J.; Cho, D.; Kwon, O. H.; Park, W. H. Silk fibroin/hydroxyapatite composite hydrogel induced by gamma-ray irradiation for bone tissue engineering. *Biomater Res* **2017**, *21*, 12.
- (20) Gibbs, D. M.; Black, C. R. M.; Dawson, J. L.; Oreffo, R. O. C. A review of hydrogel use in fracture healing and bone regeneration. *J. Tissue Eng. Regen. Med.* **2016**, *10*, 187–198.
- (21) Seliktar, D. Designing cell-compatible hydrogels for biomedical applications. *Science* **2012**, *336*, 1124–1128.
- (22) Asamura, S.; Mochizuki, Y.; Yamamoto, M.; Tabata, Y.; Isogai, N. Bone Regeneration Using a Bone Morphogenetic Protein-2 Saturated Slow-Release Gelatin Hydrogel Sheet Evaluation in a Canine Orbital Floor Fracture Model. *Ann. Plast. Surg.* **2010**, *64*, 496–502.
- (23) Ben-David, D.; Kizhner, T. A.; Kohler, T.; Müller, R.; Livne, E.; Srouji, S. Cell-scaffold transplant of hydrogel seeded with rat bone marrow progenitors for bone regeneration. *J Craniomaxillofac Surg* **2011**, *39*, 364–371.
- (24) Sachlos, E.; Czernuszka, J. T. Making tissue engineering scaffolds work. Review: the application of solid freeform fabrication technology to the production of tissue engineering scaffolds. *Eur Cell Mater* **2003**, *5*, 29–40.
- (25) Hulbert, S. F.; Morrison, S. J.; Klawitter, J. J. Tissue Reaction to Three Ceramics of Porous and Non-Porous Structures. *J. Biomed. Mater. Res.* **1972**, *6*, 347–374.
- (26) Bose, S.; Roy, M.; Bandyopadhyay, A. Recent advances in bone tissue engineering scaffolds. *Trends Biotechnol.* **2012**, *30*, 546–554.
- (27) Danilevicius, P.; Rezende, R. A.; Pereira, F. D. A. S.; Selimis, A.; Kasyanov, V.; Noritomi, P. Y.; da Silva, J. V.; Chatziniokolaidou, M.; Farsari, M.; Mironov, V. Burr-like, laser-made 3D microscaffolds for tissue spheroid encagement. *Biointerphases* **2015**, *10*, No. 021011.
- (28) Shakir, M.; Zia, I.; Rehman, A.; Ullah, R. Fabrication and characterization of nanoengineered biocompatible n-HA/chitosan-tamarind seed polysaccharide: Bio-inspired nanocomposites for bone tissue engineering. *Int. J. Biol. Macromol.* **2018**, *111*, 903–916.
- (29) Sahraee, S.; Milani, J. M.; Ghanbarzadeh, B.; Hamishehkar, H. Physicochemical and antifungal properties of bio-nanocomposite film based on gelatin-chitin nanoparticles. *Int. J. Biol. Macromol.* **2017**, *97*, 373–381.
- (30) Manna, P. J.; Mitra, T.; Pramanik, N.; Kavitha, V.; Gnanamani, A.; Kundu, P. P. Potential use of curcumin loaded carboxymethylated guar gum grafted gelatin film for biomedical applications. *Int. J. Biol. Macromol.* **2015**, *75*, 437–446.
- (31) Suzawa, Y.; Kubo, N.; Iwai, S.; Yura, Y.; Ohgushi, H.; Akashi, M. Biomimetic/Agarose Composite Gels Enhance Proliferation of Mesenchymal Stem Cells with Osteogenic Capability. *Int. J. Mol. Sci.* **2015**, *16*, 14245–14258.
- (32) Watari, F.; Takashi, N.; Yokoyama, A.; Uo, M.; Akasaka, T.; Sato, Y.; Abe, S.; Totsuka, Y.; Tohji, K. Material nanosizing effect on living organisms: non-specific, biointeractive, physical size effects. *J. R. Soc., Interface* **2009**, *6*, S371–S388.
- (33) Okada, S.; Ito, H.; Nagai, A.; Komotori, J.; Imai, H. Adhesion of osteoblast-like cells on nanostructured hydroxyapatite. *Acta Biomater.* **2010**, *6*, 591–597.
- (34) Zhou, J.; Wei, F.; Ma, Y. Inhibiting PPAR γ by erythropoietin while upregulating TAZ by IGF1 synergistically promote osteogenic differentiation of mesenchymal stem cells. *Biochem. Biophys. Res. Commun.* **2016**, *478*, 349–355.
- (35) Wei, J.; Shimazu, J.; Makinistoglu, M. P.; Maurizi, A.; Kajimura, D.; Zong, H.; Takarada, T.; Lezaki, T.; Pessin, J. E.; Hinoi, E.; Karsenty, G. Glucose Uptake and Runx2 Synergize to Orchestrate Osteoblast Differentiation and Bone Formation. *Cell* **2015**, *161*, 1576–1591.

(36) Zhang, J.; Zhang, C. F.; Li, Q. L.; Chu, C. H. Cyclic Adenosine Monophosphate Promotes Odonto/Osteogenic Differentiation of Stem Cells from the Apical Papilla via Suppression of Transforming Growth Factor Beta 1 Signaling. *J Endod* **2019**, *45*, 150–155.

(37) Ionescu, A. M.; Drissi, H.; Schwarz, E. M.; Kato, M.; Puzas, J. E.; McCance, D. J.; Rosier, R. N.; Zuscik, M. J.; O'Keefe, R. J. CREB Cooperates with BMP-stimulated Smad signaling to enhance transcription of the Smad6 promoter. *J. Cell. Physiol.* **2004**, *198*, 428–440.

(38) Khan, K.; Pal, S.; Yadav, M.; Maurya, R.; Trivedi, A. K.; Sanyal, S.; Chattopadhyay, N. Prunetin signals via G-protein-coupled receptor, GPR30(GPER1): Stimulation of adenylyl cyclase and cAMP-mediated activation of MAPK signaling induces Runx2 expression in osteoblasts to promote bone regeneration. *J Nutr Biochem* **2015**, *26*, 1491–1501.

(39) Siddappa, R.; Mulder, W.; Steeghs, I.; van de Klundert, C.; Fernandes, H.; Liu, J.; Arends, R.; van Blitterswijk, C.; de Boer, J. cAMP/PKA signaling inhibits osteogenic differentiation and bone formation in rodent models. *Tissue Eng Part A* **2009**, *15*, 2135–2143.

(40) Tintut, Y.; Parhami, F.; Le, V.; Karsenty, G.; Demer, L. L. Inhibition of osteoblast-specific transcription factor Cbfa1 by the cAMP pathway in osteoblastic cells. Ubiquitin/proteasome-dependent regulation. *J Biol Chem* **1999**, *274*, 28875–28879.

(41) Lennon, D. P.; Haynesworth, S. E.; Young, R. G.; Dennis, J. E.; Caplan, A. I. A chemically defined medium supports in vitro proliferation and maintains the osteochondral potential of rat marrow-derived mesenchymal stem cells. *Exp. Cell Res.* **1995**, *219*, 211–222.